Structure and electronic properties of graphite nanoparticles

Odd E. Andersson, B. L. V. Prasad, Hirohiko Sato, and Toshiaki Enoki*
Department of Chemistry, Tokyo Institute of Technology, 2-12-1 Ookayama, Meguro-ku, Tokyo 152-8551, Japan

Yoshihiro Hishiyama and Yutaka Kaburagi
Faculty of Engineering, Musashi Institute of Technology, 1-28-1 Tamazutsumi, Setagaya-ku, Tokyo 158-8557, Japan

Masanori Yoshikawa
Department of Control and System Engineering, Tokyo Institute of Technology, 2-12-1 Ookayama, Meguro-ku, Tokyo 152-8551, Japan

Shunji Bandow
Japan Science and Technology Corporation, Department of Physics, Meijo University, 1-501 Shiogamaguchi, Tempaku-ku, Nagoya 468-8502, Japan
(Received 4 May 1998)

We have investigated the structure and electronic properties of graphite nanoparticles prepared by heat treating diamond nanoparticles. The prepared nanographite forms a polyhedron with a hollow in its inside, whose faces comprise a stacking of 3–6 planar graphene sheets with an in-plane size of 7–8 nm and an intersheet distance of 0.353 nm. The large intersheet distance suggests a considerably large reduction in interlayer interaction compared to the case of bulk regular graphite. Electron-spin-resonance and magnetic-susceptibility measurements show that there is a considerable enhancement in the density of states at the Fermi energy, indicating the presence of an additional band superimposed upon the bonding π and the antibonding π^* bands around the Fermi energy. Taking into consideration the discontinuous shape at an edge line formed by crossing adjacent graphene sheets, graphene sheets in a nanographite particle are considered to have open π-bond edges. On the basis of the theoretical suggestion that nonbonding π orbitals give edge-inherited surface states depending on the shape of the graphene edge, this is suggestive of the contribution of the edge states to the electronic structure of nanosized graphene having open π-bond edges. [S0163-1829(98)07948-X]

I. INTRODUCTION

Recently, fullerenes and carbon nanotubes have been targeted for intensive studies due to their interesting electronic properties related to nanosized systems.[1] In these materials, π-conjugated carbon hexagon rings are condensed to form a closed surface with the participation of pentagon rings. Because of their specific sizes, which are in between ordinary molecules and bulk solids, they show interesting features in their electronic properties in relation to quantum size effects.[2–4] In addition, graphite nanoparticles give another aspect in carbon-based nanoparticles having conjugated π-electron systems. When a graphite crystal is cut into nanoparticles, there appear edges which surround the graphite particles. A graphite nanoparticle consists of a stacking of nanosized graphene sheets whose peripheries are formed with σ dangling bonds to which, in actual cases, foreign chemical species such as hydrogen or oxygen tend to react in the atmosphere, resulting in completed bonds. In this sense, a nanographite is characterized by finite flat graphene sheets having open edges, whereas fullerenes and carbon nanotubes have closed surfaces. Therefore, the presence of open edges around the peripheral region adds specific features to nanographite systems which are different from their closed-surface counterparts, such as fullerenes and carbon nanotubes. Recently, Tanaka *et al.*[5] and Fujita and co-workers[6–8] theoretically suggested that the electronic structures of finite-size graphene sheets depend crucially on the shape of their edges. The graphene edge of an arbitrary shape comprises two types of edges, zigzag type and armchair type, where the former has a *trans*-polyacetylene type structure while the latter has a *cis*-polyacetylene one. According to theoretical suggestions, nonbonding π levels appear around the Fermi energy in the case of zigzag-type edges, whereas no nonbonding levels of this kind exist in armchair-shaped edges. As a consequence, the presence of a nonbonding π band gives interesting electronic properties associated with electrons in the nonbonding band which tend to be localized around the peripheral region. In this respect, an investigation of graphite nanoparticles will give important information about the edges of nanosized open-edged graphene sheets.

In connection with carbon-based nanoparticles, nanosized diamond particles have been known to be prepared by explosion-induced high-pressure techniques, where they have a regular atomic arrangement of a diamond structure with sizes of $\sim$5 nm.[9,10] Heat treatment above $\sim$1000 °C converts diamond into graphite. Accordingly, it is interesting to prepare graphite nanoparticles by the heat treatment of diamond nanoparticles. In this paper, we present structures and electronic properties of graphite nanoparticles prepared from diamond nanoparticles which are investigated by means of scanning electron microscopy, electron microscopy, x-ray diffraction, Raman scattering, electron-spin resonance (ESR), and magnetic susceptibility. The experimental

findings suggest that the prepared nano-graphite forms a polyhedron whose faces comprise a stacking of 3–6 planar graphene sheets with an in-plane size of 7–8 nm. The electronic density of states is found to be considerably enhanced due to the presence of the edge-inherited nonbonding π orbitals at the Fermi level, consistent with theoretical suggestions.

II. EXPERIMENTAL DETAILS

Graphite nanoparticles were prepared by graphitization of nanodiamond powder [Cluster Diamond, Toron Company Ltd. (grain size 4–6 nm)] in an inert argon atmosphere. The mean size and the size distribution of the diamond particles checked by transmission electron microscopy were in good agreement with the reported ones (catalogue specifications). In order to avoid contamination with magnetic impurities, we treated nanodiamond particles by soaking in concentrated HCl before use. However, there was no appreciable change in the observed magnetic properties after acid treatment. 20–50 mg of pristine nanodiamond powder placed in a graphite crucible was heat treated in a graphite furnace in an argon atmosphere. To investigate the temperature dependence of the graphitization process, we employed 1600, 1700, 1800, and 2750 °C for heat-treatment temperatures, where the lowest limit was based on the results of Evans and James.[11] The holding time at the temperature was 1 h for heat treatment temperatures (HTT's), 1600, 1700, and 1800 °C, and 30 min for a HTT of 2750 °C. The shorter holding time at 2750 °C is due to the shorter lifetime of the furnace at this temperature. The structure of the obtained particles was characterized by means of transmission electron microscopy, scanning electron microscopy, x-ray powder diffraction and Raman scattering. A transmission electron microscope observation was carried out using a Phillips EM400 instrument with the acceleration voltage of 120 kV, while scanning electron microscope pictures were taken using a Hitachi S900 instrument with an acceleration voltage of 5 kV. X-ray-diffraction profiles were obtained by a Rigaku RINT-2400 instrument with a Cu target (50 kV, 120 mA). Silicon powder was used to calibrate the diffraction peaks that were obtained. Raman-scattering experiments were carried out with Jobin-Yvon T64000 instrument together with an argon-ion laser ($\lambda = 514.5$ nm), using a backscattering microprobe technique. Electronic and magnetic properties were investigated by means of ESR and magnetic susceptibility. ESR spectra were measured with a conventional *X*-band spectrometer (JEOL JES-TE20) in the temperature range 2–300 K, where the magnetic field and microwave frequency were calibrated using a NMR gaussmeter and a frequency counter, respectively. ESR intensities and spin-lattice relaxation times were calibrated using DPPH as a reference. ESR saturation curves were taken up to the maximum microwave power of 200 mW for the estimation of spin-lattice relaxation times.[12] The magnetic susceptibility and magnetization were measured with Quantum Design MPMS-5 DC-SQUID (superconducting quantum interference device) susceptometer in the temperature range 1.6–300 K under magnetic fields up to 5 T.

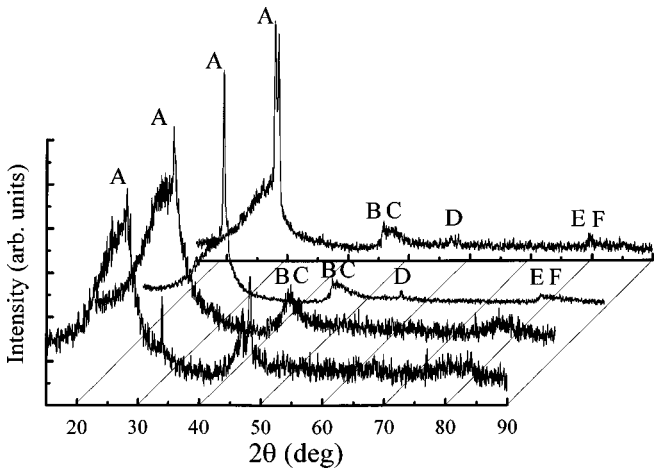

FIG. 1. X-ray diffractograms of samples heat treated at 1600 °C, 1700 °C, 1800 °C, and 2750 °C. *A*, *B*, *C*, *D*, *E*, and *F* are diffraction peaks indexed to (002), (100), (101), (004), (110), and (112), respectively.

III. RESULTS

Figure 1 shows the x-ray diffractograms of the 1600, 1700, 1800, and 2750 °C heat-treated samples. The 1600 °C HTT sample shows very broad peaks at the graphite (002), (100), (101), (110), and (112) positions, as well as additional sharp peaks corresponding to the diamond (111) peak and impurities (~45°), where graphite (100) and (101) peaks merge into a single broad peak around 45°, and graphite (110) and (112) peaks around 80°. The (002) peak has an asymmetric shape with a steep high angle tail. The 1700 °C HTT sample shows the coexistence of a very broad peak and a relatively sharp peak at the graphite (002) position around 26°, in addition to a broad peak at 42°–44° corresponding to the graphite peaks (100) and (101). For the 1800 °C HTT sample, the sharp peak at 26° is more pronounced, indicating that the crystallite size becomes larger in the *c*-axis direction, although the shoulder-shaped broad feature still survives on the low-angle side of the sharp peak. This is also shown in the sharper (100) and (101) peaks, where a broad shoulder contributes on the high-angle side of the sharp feature. For the sample heat treated at 1800 °C, we can clearly see peaks of graphite (004), (110), and (112). Increasing the heat treatment temperature to 2750 °C does not result in any major change in the x-ray diffractogram, except that the narrow peak at 26° now splits into two peaks. The experimental findings suggest the presence of two kinds of graphitic regions having different sizes, where the large-size graphitic region develops much more as the heat treatment temperature is raised. At the same time, the sample heat treated at the lowest temperature of 1600 °C involves a trace of nanodiamond as a minority phase. On the basis of the x-ray diffractograms, we investigated further the sample heat treated at 1700 °C, as a target for the electronic properties of nanosized graphite particles, since this sample is well graphitized with the features of nanoparticles and there is only a small amount (~20%) of large-sized particles (see Table I), where the amount of large-sized particles is estimated from the ratio between integrated intensities of broad and narrow peak contributions assigned to the graphite (002) peak.

Here, in order to estimate the sizes *L* of the obtained

TABLE I. Fitted parameters for the x-ray-diffraction profiles for the sample heat treated at 1700 °C. The peak around 26° is deconvoluted into (002) narrow and broad peaks, and that around 43°–47° into (100) and (101) peaks.

Peak	Area (arb. units)	Amplitude (arb. units)	Position (deg)	Width (deg)
(002) narrow	0.019	0.023	26.035	0.515
(002) broad	0.074	0.012	25.131	4.067
(100)	0.032	0.016	43.226	1.308
(101)	0.069	0.016	44.768	2.838

graphite nanoparticles, the intensities of that sample were corrected for the Lorentz-polarization factor

$$LP(\theta)=(1+\cos^2 2\theta)/\sin^2\theta\cos\theta, \tag{1}$$

the atomic form factor $f(\theta)$, and the factor

$$A(\theta)=\mu/2[1-\exp(-2\mu t/\sin\theta)], \tag{2}$$

where μ is the absorption coefficient and t is the thickness of the sample. The total correction of the intensities is then given by the equation

$$I_{\text{corrected}}=I_{\text{observed}}/LP(\theta)\times f^2(\theta)\times A(\theta). \tag{3}$$

In Fig. 2 we show the corrected (002), (100), and (101) peaks of the graphite sample heat treated at 1700 °C. The (002) peak of graphite was then fitted to two Lorentzian functions, one for the broad peak and one for the narrow peak. In the same way, Lorentzian functions were fitted to the (100) and (101) peaks. The fitted parameters are given in Table I. Using these values and a standard silicon powder sample as a reference, we estimate the thickness and the in-plane size of the particle grains. For the broad graphite (002) peak, we find a grain thickness of $t\approx 2.2$ nm, and for the narrow peak a grain thickness of $t\approx 19.3$ nm. The intensity of the (100)/(101) peak is so weak that it is difficult to make sure if two kinds of peaks with different peak widths are present or not for each in-plane diffraction peak assigned to (100) or (101). Thus, in this case, we deconvolute the broad feature around 43°–47° into single (100) and (101) peaks on the assumption that each peak originates mostly from a single component. The obtained contribution to the (100) peak summarized in Table I gives an estimate of the in-plane size of $L_a\approx 8$ nm. From the locations of peak centers for the broad and narrow *c*-axis diffraction (002) peaks at 25.13° and 26.04°, respectively, the interlayer distances between graphene sheets are estimated at 0.353 and 0.342 nm, which are considerably longer than the interlayer distance of 0.3354 nm for bulk regular graphite. Judging from the sample thickness in addition to the intergraphene sheet distances, the number of graphene sheets are estimated at ~56 and ~6 for larger and smaller particles, respectively.

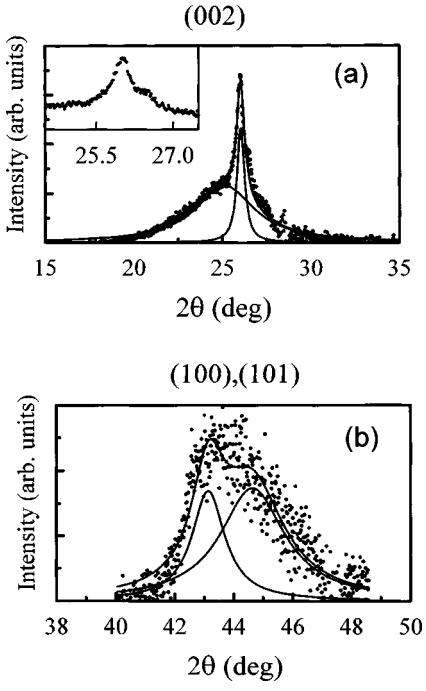

FIG. 2. (a) Fittings of the (002) peak to two Lorentzian functions (solid lines) with different widths for the sample heat treated at 1700 °C. The inset shows the detailed feature with high angle resolution. (b) Fitting of the combined peak profile of (100) and (101) peaks to two Lorentzian functions (solid lines) corresponding to (100) and (101) diffraction lines for the sample heat treated at 1700 °C.

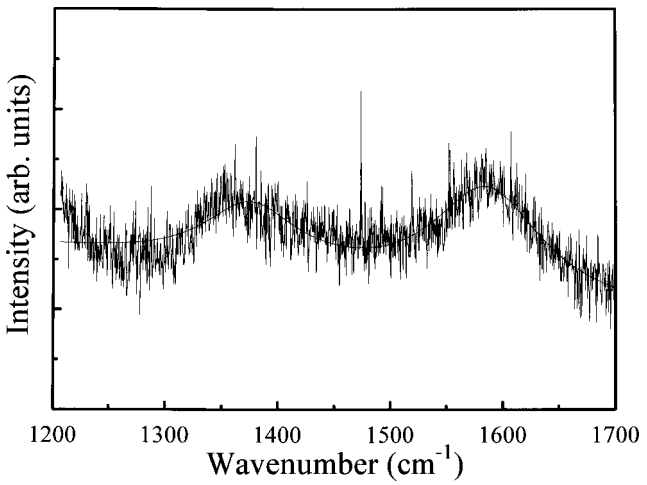

FIG. 3. Raman-scattering spectrum of the samples heat treated at 1700 °C. The solid line is a fitting curve with two Lorentzian functions.

Figure 3 shows the results of the Raman scattering experiment for the sample heat treated at 1700 °C. The Raman-scattering spectrum reveals two broad peaks at around 1570 and 1350 cm^{-1} which are assigned to the E_{2g2} and disorder-induced modes of graphite, respectively, consistent with the finite size of the particles. Using the empirical formula $L_a\approx 4.4\times I_{1570}/I_{1350}$,[13] where I_{1570} and I_{1350} are the intensities of the peaks corresponding to the E_{2g2} and disorder-induced modes, respectively, we estimate the in-plane size at $L_a\approx 7.6$ nm, which is consistent with the x-ray analysis mentioned above.

Scanning electron microscopy is not really suited for observing nanosized materials. However, it gives good information about the morphology of the samples and the formation of large-sized particles as well. Scanning electron microscope observations suggest that the pristine diamond is a very uniform sample composed of nanoparticles of the

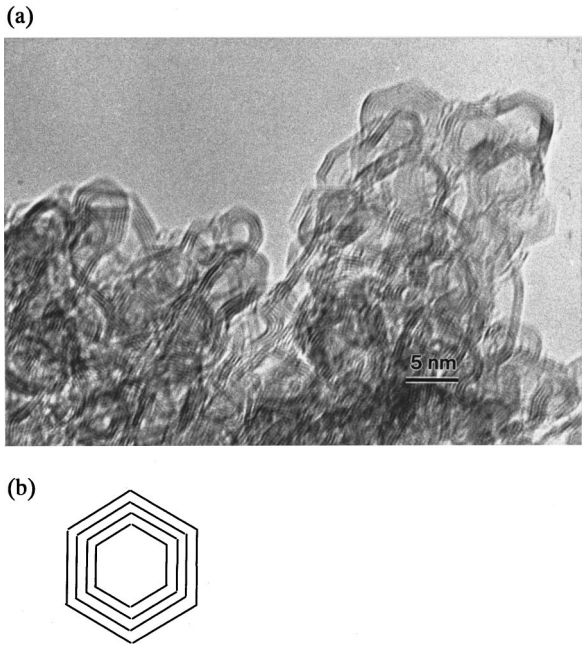

FIG. 4. (a) Transmission electron microscope picture of the sample heat treated at 2750 °C. (b) A schematic picture of a typical graphite nanoparticle polyhedron.

same particle size. The sample heat treated at 1600 °C is also very uniform with only nanometer-sized particles, though pristine diamond particles are evidenced as a minority phase by x-ray diffraction. At 1700 °C and 1800 °C heat treatment temperatures, we have some larger-sized graphite particles having particle sizes of ~200–500 nm in addition to the nanosized particles. This is consistent with the x-ray-diffraction experiments. For samples heat treated at 2750 °C, larger-sized particles become major ingredients whose sizes are roughly in the same range as those for 1700 and 1800 °C HTT's.

Figure 4 shows a transmission electron microscope picture of the sample heat treated at 2750 °C. The structural features of the heat-treated particles are in good agreement with the experimental findings in the x-ray-diffraction and Raman-scattering spectra. Individual nanoparticles are likely to have polyhedron-shaped crystal habits, whose surfaces are formed with a stacking of ~3–6 graphene sheets. Closed surfaces of graphene multilayers show a hollow inside each particle, resulting in onion-shaped carbon polyhedra. These nanosized polyhedra are present in all samples heat treated at different temperatures between 1600 and 2750 °C. The size is independent of the heat treatment temperature, in addition to the absence of any morphological difference. However, at the higher heat treatment temperatures there is a larger amount of large-sized graphite particles, having sizes larger than 100 nm.

Figure 5 shows the result of the ESR investigation on the HTT1700 sample. The ESR spectra reveal two Lorentzian signals. At temperatures above ~170 K we have one broad signal with a linewidth $\Delta H \approx 3.7$ mT at 295 K. Below 170 K, a second narrow signal appears with $\Delta H = 0.4-0.5$ mT. The g values are estimated at $g = 2.0014$ and 2.0010 for the broad and narrow signals, respectively. The small values for the linewidths and the small deviation of the g values from the

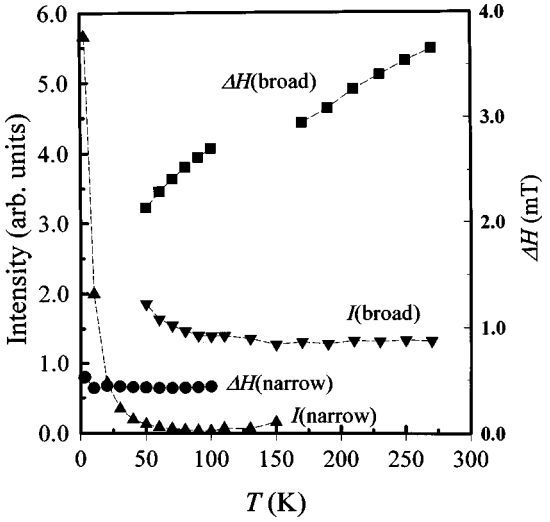

FIG. 5. Temperature dependence of the intensity I and the linewidth ΔH for the narrow and broad signals in the ESR spectra of the 1700 °C heat-treated sample.

free-electron-spin g value suggest that the observed spins originate not from transition-metal magnetic impurities but from carbon-inherited spin species in the graphite nanoparticles. In the temperature range above ~80 K, below which the coexistence of the narrow and broad signals makes the analysis ambiguous, the intensity of the broad signal is essentially independent of temperature, which gives a value of the spin susceptibility of $\chi_s = 2.8 \times 10^{-7}$ emu/g. The intensity of the narrow signal shows a Curie-type temperature dependence, where, fitting the data for the narrow signal to the Curie law, we obtain a concentration for the localized spins $N = 5 \times 10^{18}$ spins/g. The linewidth of the broad peak decreases with decreasing temperature. The superposition of the narrow signal upon the broad signal makes the estimation of the linewidth rather difficult in a temperature range below about 150 K. Thus the discontinuity appearing between 150 and 110 K is artificial due to the ambiguity of the analysis. The linewidth is halved when the temperature is lowered from room temperature to 4.2 K. The linewidth of the narrow signal is independent of temperature over the whole temperature range investigated. No ESR saturation effect is observed for the broad signal up to the maximum microwave power of 200 mW, suggesting that the spin-lattice relaxation time is shorter than at least 10^{-6} s.

Magnetic-susceptibility and magnetization measurements give complementary information on the magnetic properties. The magnetization curve shows the absence of residual magnetization at $H = 0$ T and $T = 5.0$ K, suggesting the absence of ferromagnetic impurities. As exhibited in Fig. 6, the feature of magnetization curve at $T = 5.0$ K is explained with the summation of a linear field-dependent term with a negative slope and a Brillouin-curve-type positive term. The linear term is associated with the combination of core diamagnetism, orbital diamagnetism, and Pauli paramagnetism. The Brillouin-curve-type term is explained with localized magnetic moments of $s = \frac{1}{2}$. These experimental findings give evidence that transition metal magnetic impurities contribute to the observed results to a negligibly small extent, taking into account the g value and the linewidth of the ESR spectra. In Fig. 7, we show the temperature dependence of mag-

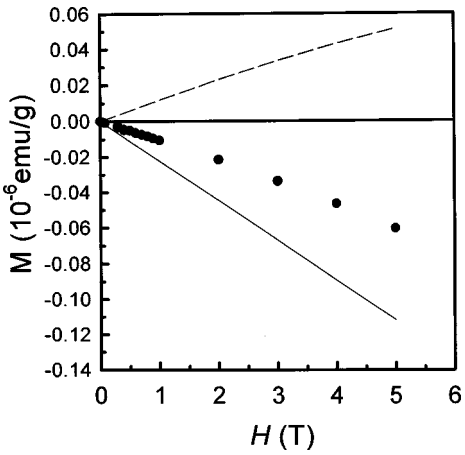

FIG. 6. The magnetization vs field plot at 5.0 K for the 1700 °C heat-treated sample. The experimental results (full circle) are explained with the summation of a linear field-dependent term with a negative slope (solid line) and a Brillouin curve with $s=\frac{1}{2}$ (dashed line).

netic susceptibility for the sample heat treated at 1700 °C. At 300 K the total magnetic susceptibility χ is -2.13×10^{-6} emu/g. The susceptibility decreases monotonically with decreasing temperature. At low temperatures below ~50 K, the susceptibility shows a Curie-like increase. The data are analyzed on the basis that the total susceptibility consists of core diamagnetism, Curie paramagnetism, orbital diamagnetism, and Pauli paramagnetism: $\chi=\chi_{\rm core}+\chi_{\rm Curie}+\chi_{\rm orb}+\chi_{\rm Pauli}$, where the Pascal rule gives $\chi_{\rm core}=-0.5\times10^{-6}$ emu/g. The Curie contribution $\chi_{\rm Curie}$ gives an estimate of the localized spin concentration $N\approx1\times10^{19}$ spins/g, in good agreement with the ESR narrow signal result.

IV. DISCUSSION

A. Structure of the graphite nanoparticle

Now we discuss the structural properties of nanographite prepared from diamond nanoparticles. The detailed structural features are summarized from the results of x-ray diffraction, Raman-scattering spectra, scanning electron microscopy and transmission electron microscopy; that is, the prepared graphite nanoparticle forms a polyhedron comprising faces of graphene multilayers (3–6 graphene sheets), where the inside of the polyhedron is a hollow. The average size of graphene sheets is in the range of 7–8 nm. The intergraphene sheet distance is estimated at 0.353 nm, which is considerably larger than that for bulk regular graphite: 0.3354 nm. The large intergraphene distance ranging around 0.353 nm suggests more than a 30% reduction in the intergraphene sheet interaction in comparison with bulk regular graphite,[14] and the strongly disordered stacking feature contributes more seriously to the reduction in the intersheet interaction, so that we can treat the graphite nanoparticles as an assembly of very weakly bound nanographene sheets. Similar structural features were obtained by Kuznetsov and co-workers for electron-beam-heated diamond nanoparticles.[15,16] In their work, the heat treatment temperature 1000–1500 °C was lower than that for the present case, giving rise to rather round-shaped particles with disorderedly wrinkled sheets. The structure of the graphite nanoparticle resembles carbon onions consisting of round-shaped closed surfaces of multiwalls which have been recently discovered.[15–18] However, the presence of edges formed by crossing lines between adjacent flat-planar-shaped graphene sheets is an important structural feature different from round-shaped carbon onions, which is understood on the basis of the structure of diamond that is used as a starting material. The {111} diamond surface having a hexagonal arrangement of carbon atoms has an almost equivalent geometry to that of the graphene hexagons, except for the fact that the former is featured by corrugated sheets. There are eight surfaces involved in the {111} surface. Diamond surfaces are unstable even at room temperature due to the presence of σ dangling bonds protruding from the surfaces, eventually resulting in a structural rearrangement with the formation of a superlattice governed by π bonding.[19,20] Accordingly, heat treatment makes the {111} planes easily converted to graphene planes. As a consequence, the projected shape of the polyhedral structure from the [110] direction and its equivalents becomes hexagonal, in good agreement with the appearance of the observed lattice image of nanoparticles as shown in Fig. 4. The 7–8-nm size of the obtained graphite nanoparticles is larger than that of the pristine diamond particles, whose typical sizes range from 4–6 nm. This is explained by the presence of hollows inside the graphite nanoparticles, and these hollows occupy 10–20 % of the total volume of a nanographite on average. Corrugated hexagons on the (111) plane of the diamond structure become flat through the formation of π-conjugated hexagons on the graphene layers after heat treatment, which brings about the extension of the in-plane size. Taking into account the difference in densities between graphite (2.25 g/cm^3) and diamond (3.52 g/cm^3), the observed increase in the particle volume in the graphitization process is reasonably understood.

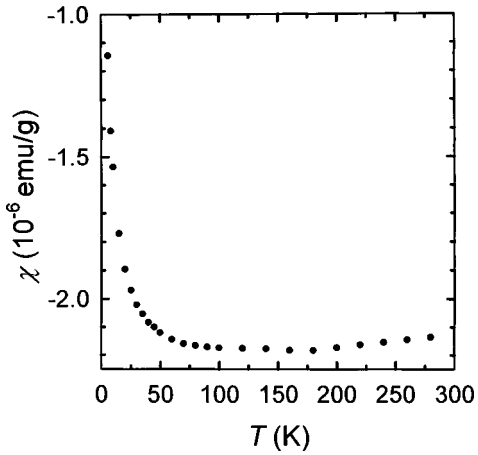

FIG. 7. Temperature dependence of the magnetic susceptibility for the 1700 °C heat-treated sample taken in the field of 1 T.

B. Edge electronic states

Next we discuss the electronic and magnetic properties of graphite nanoparticles. The results of ESR and magnetic susceptibility suggest two kinds of paramagnetic species. One of them corresponds to the Curie contribution as observed in the narrow ESR signal and the Curie tail in the temperature dependence of magnetic susceptibility, where the concentra-

tion of localized spins is estimated at $\sim 1\times 10^{19}$/g. The independence of the narrow ESR signal from the broad one and the temperature-independent linewidth for the narrow signal demonstrate that the localized spins are isolated from their surroundings. Consequently, they are considered to be assigned to localized spins associated with defects independent of the graphite π electrons. The observed spin concentration proves that each graphite nanoparticle has, on average, one localized spin of defect origin, according to the information on the size of the nanoparticles which gives the mean weight of a single particle of $\sim 10^{-19}$ g. The ESR broad signal is considered to be assigned to π-electron spins, since the graphite electronic structure around the Fermi level is governed by π-electron bands. The magnetic susceptibility ascribed to the broad signal is independent of temperature, showing a feature characteristic of Pauli paramagnetism.

Here we extract information on the electronic structure from the results of the magnetic susceptibility. In the magnetic susceptibility after the correction of the Curie and core terms, there are two other contributions; the Pauli paramagnetic contribution and the orbital diamagnetic contribution. A graphite nanoparticle is considered to consist of finite-size graphene sheets weakly interacting with adjacent sheets on the same polyhedron surface. Therefore, π electrons are scattered around graphene boundaries. The electronic feature thus characterized with the carrier scattering is interpreted as disordered graphite, which Kotosonov theoretically analyzed in terms of the modified version of the Slonczewski-Weiss-McClure model for the orbital diamagnetism, as expressed in the following equation:[21,22]

$$\chi_{\rm orb} = -\frac{4.6\times 10^{-3}\ \mathrm{sech}^2\{E_F/2k_B(T+\Delta T)\}}{T+\Delta T}, \qquad (4)$$

where E_F is the Fermi energy, k_B is the Boltzmann constant, and the Dingle temperature ΔT is related to the scattering time τ associated with disorder scattering as given by $\Delta T \approx \hbar/\pi k_B \tau$. Here, if we assume that the scattering is governed by the particle boundary scattering $\tau \approx \tau_b$, the scattering time is expressed in terms of the Fermi velocity v_F and the particle size L,[22]

$$\tau_b = \frac{L}{v_F}, \qquad (5)$$

where the Fermi velocity $v_F \approx 9.7\times 10^5$ m/s for bulk regular graphite π bands is employed since the Fermi velocity does not depend on the location of the Fermi level in the linear k-dependent energy dispersion of the graphite π-electron energy band.[23] (The energy discreteness expected for the quantum size effect of the present nanoparticles involving typically $\sim 10^3$ carbon atoms is in the range of $\sim$10 K, which is estimated from the graphite band width $\sim$3 eV,[23] giving a minor effect on the orbital susceptibility.) Using the observed in-plane size of the graphite nanoparticles $L_a \approx 7-8$ nm, the scattering time is estimated at $\tau_b \approx 7\times 10^{-15}$ s, resulting in $\Delta T \approx 390$ K. The Fermi energy is adjusted in such a manner that the slope of the observed susceptibility vs temperature plot above 150 K is reproduced since it originates from the orbital susceptibility and is sensitive to the value of the Fermi energy. The best fitting of the observed slope to the temperature dependence in Eq. (4) gives $E_F \approx 0.082$ eV. (As we will discuss later, the presence of nonbonding π states located around E_F, that is specific for graphite nanoparticles, has to be taken into account in the calculation of the orbital susceptibility. However, the nonbonding states well localized around the particle edges are considered not to contribute to such a large extent that the present discussion becomes invalid.) The calculated orbital diamagnetic susceptibility as a function of temperature is given in Figs. 8 and 9 in addition to other susceptibility

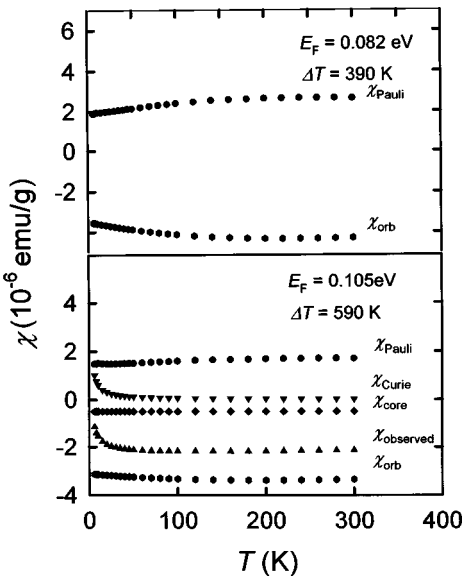

FIG. 8. The contributions of the Pauli paramagnetism, the Curie paramagnetism, the orbital diamagnetism, and the core diamagnetism to the observed susceptibility. The orbital susceptibility is calculated with the two sets of values for the Fermi energy and the Dingle temperature: $E_F = 0.082$ eV and $\Delta T = 390$ K, and $E_F = 0.105$ eV and $\Delta T = 590$ K.

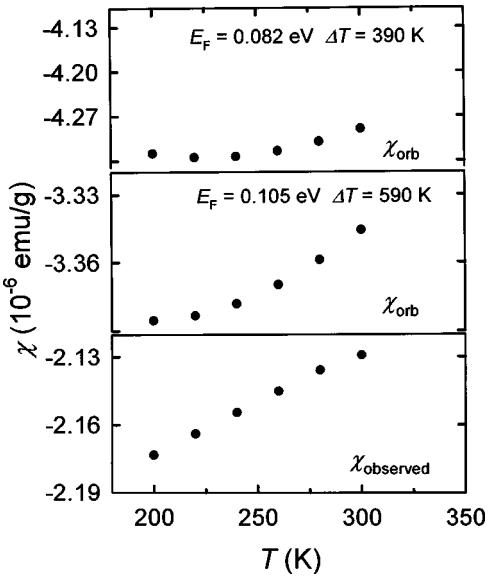

FIG. 9. The detailed behavior of the calculated orbital susceptibility using two sets of fitting parameters for the Fermi energy and the Dingle temperature, $E_F = 0.082$ eV and $\Delta T = 390$ K, and $E_F = 0.105$ eV and $\Delta T = 590$ K, compared with the observed susceptibility above 200 K.

contributions. The observed susceptibility decreases monotonically as the temperature is lowered in a high-temperature range above about 150 K. The slope of the susceptibility vs temperature curve is not well reproduced in the calculated orbital diamagnetic susceptibility even in the best fitting with $E_F = 0.082$ eV, as shown in Fig. 9. After the subtraction of the orbital susceptibility, we obtain the Pauli paramagnetic susceptibility χ_{Pauli} as the remaining constituent, which corresponds to the broad ESR signal. The absolute value of the Pauli paramagnetic susceptibility is estimated at 2.6×10^{-6} emu/g at room temperature from the observed magnetic susceptibility, but some temperature dependence appears at low temperatures which is caused by an artifact of the fitting due to the inappropriateness of the chosen value. In order to try to reduce the effect, we take another choice of ΔT, with the value of $\Delta T \approx 590$ K from the information of nanographites in activated carbon fibers which are considered to have a similar particle size to that of the present graphite nanoparticles.[22] In this case, the artificial temperature dependence is eliminated in the Pauli paramagnetic contribution with $E_F \approx 0.105$ eV and $\chi_{\mathrm{Pauli}} \approx 1.7 \times 10^{-6}$ emu/g at room temperature, and the slope is roughly reproduced above 200 K, as shown in Fig. 9. The obtained values of the Pauli paramagnetic susceptibility are not so different between the two choices of ΔT. Consequently, the above calculations suggest that the absolute value of the orbital susceptibility is rather insensitive to the value of the Fermi energy if it is around 0.1 eV. Moreover, the weak temperature dependence of the orbital susceptibility in the temperature range above 200 K is considered to be associated with the small Fermi energy.

The ESR broad signal gives an estimate of 2.8×10^{-7} emu/g for the Pauli paramagnetic contribution which is about one order of magnitude smaller than that estimated from the magnetic susceptibility. The difference is considered to be caused not only by the calculation of the ESR intensity but also by the ambiguous estimation of the orbital diamagnetic susceptibility on the basis of the values of the Fermi energy and the disorder-induced scattering time. The presence of large-size particles, whose amount is $\sim$20%, introduces another factor that has to be considered in more quantitative calculations. However, it is worth noting that the values of the observed Pauli paramagnetic susceptibility are one or two orders of magnitudes larger than the Pauli contribution expected for bulk regular graphite, with $\chi_{\mathrm{Pauli}} \approx 2 \times 10^{-8}$ emu/g, that is estimated from $E_F \approx 0.082 - 0.105$ eV.[23,24] This means a considerably large enhancement in the density of states at the Fermi energy compared with bulk regular graphite, where the Fermi energy is placed around the minimum in the density of states between the bonding π and antibonding π^* bands. Therefore, the enhanced density of states suggests the presence of an additional band superimposed upon the ordinary graphene π and π^* bands around the Fermi energy. There are two possibilities for the assignment of the additional band, dangling bonds of σ orbital origin and a nonbonding π orbital, the latter of which was theoretically suggested by Tanaka *et al.*[5] and Fujita and co-workers.[6–8] The sample was handled in air, so that σ dangling bonds are considered to be saturated with foreign atoms such as oxygen and hydrogen through oxidation due to their strong chemical activity, resulting in a magnetically silent feature of the σ bonds. It will also be plausible that dangling bonds at the edges of adjacent graphene sheets are cross-linked to each other, and are eventually eliminated at the regions to which foreign atoms are not accessible. Moreover, even if spins of σ dangling bonds exist, they are expected to behave as localized magnetic moments having a Curie-type feature, since they do not interact with surrounding π and σ electrons which are considered to occupy the orbitals orthogonal to the dangling-bond orbital. Therefore, the observed temperature-independent feature in the paramagnetic susceptibility is not in agreement with that expected above.

The other possibility is related to nonbonding π orbitals. A nanographite sheet of an arbitrary shape has a periphery consisting of zigzag- and armchair-type edges where the ratio between these edges varies depending on the edge shape. An armchair-type edge does not add any additional features to the electronic structure of graphene, whereas an edge-inherited π state appears in the case of the periphery having a zigzag shape. The edge π states are suggested to be located between the π bonding and π^* antibonding bands as nonbonding states, where electrons in the states are localized around the marginal region of a nanographene sheet. Consequently, the presence of the edge states on zigzag edges around the Fermi energy makes an additional contribution to the density of states, resulting in the enhancement in the Pauli paramagnetic susceptibility. In other words, the enhanced paramagnetic susceptibility strongly proves the presence of the edge-inherited nonbonding π levels around the Fermi energy, although the participation of cross-linking bonds between adjacent graphene sheets will modify the features of the edge states in the present case where an edge corresponds to the open π-bond edge formed by crossing adjacent graphene sheets; that is, it separates an extended π-electron region into two subregions. This interesting electronic structure of the edge origin is associated with the nanosized features of the particles investigated, taking into account that the edge states are mostly emphasized in nanometer-sized particles according to the theoretical suggestions.[7] In this connection, it should be remembered that the graphite nanoparticles, prepared from diamond nanoparticles which consist of faces of planar graphene sheets, are different from fullerenes and carbon onions formed with spherical closed cages of a carbon hexagon network with an admixture of a small number of pentagon rings.

C. Spin-lattice relaxation

Finally, we discuss the origin of the linewidth for the broad ESR signal assigned to π electrons. The linewidth decreases monotonically as the lowering of the temperature. At liquid helium temperature it goes to $\Delta H \approx 20$ G. No power saturation in the microwave power saturation measurement is observed up to 200 mW, which suggests that the spin-lattice relaxation time T_1 is shorter than 10^{-6} s. Taking into consideration the Lorentzian line shape, the motional narrowing effect suppresses the contribution of the spin-spin relaxation process to the linewidth, similar to the case of conduction electrons in ordinary metals. In other words, the linewidth is governed by the spin-lattice relaxation process. According to theoretical suggestion,[2] the linewidth associated with the

spin-lattice relaxation in an ordinary conduction carrier system (Elliott mechanism) is expressed by the equations,

$$\Delta H \approx \frac{\hbar}{2\sqrt{3} g \mu_B T_1}, \tag{6}$$

$$\frac{1}{T_1} \approx \alpha (\Delta g)^2 \left(\frac{1}{\tau_b} + \frac{1}{\tau_p} \right), \tag{7}$$

where α is a numerical factor whose magnitude is on the order of 1, μ_B is the Bohr magneton, and Δg is the deviation of the g value from the free-electron spin g value (2.0023). τ_b and τ_p are the scattering times associated with electron-scattering events by particle boundaries and phonons, respectively, where the former is temperature independent and the latter is temperature dependent and gives no contribution at $T=0$ K. τ_b is given by Eq. (5), and τ_p is related to the electron mean free path l_p caused by the electron-phonon interaction:

$$\tau_p = \frac{l_p}{\nu_F}. \tag{8}$$

Using the estimated value of τ_b and the observed g-value deviation $\Delta g = g - g_0 \approx -1.0 \times 10^{-3}$, T_1 is calculated at $\sim(7-8)\times 10^{-9}$ s for particle boundary scattering, where we assume $\alpha \approx 1$. Meanwhile, the ESR linewidth at $T=0$ K gives the observed relaxation time $T_1 \approx 0.47 \times 10^{-9}$ s through the relation between ΔH and T_1 given in Eq. (6). Consequently, the observed relaxation time at $T=0$ K is semiquantitatively explained on the basis of the particle boundary scattering process. Here, since nonbonding edge states are considered to interact with π and π^* electronic states, it should be noted that the resulting modification of the electronic structure around the Fermi energy contributes to the difference between the experimentally obtained result and the theoretical prediction.

We attribute the temperature-dependent term in the linewidth to the phonon contribution according to Eq. (7). It is very surprising that the graphite nanoparticles have a temperature-dependent feature in the linewidth, because, in ordinary nanoparticles, the electron mean free path associated with phonon scattering is apt to be larger than the particle size, resulting in ineffectiveness of the phonon scattering. Graphite has two kinds of phonon modes which contribute to the electron-phonon process, longitudinal acoustic in-plane and out-of-plane modes, where the energy of the in-plane mode (Debye temperature $\sim$2480 K) is about one order of magnitude larger than that of the out-of-plane one (Debye temperature $\sim$180.5 K), since the former is related to the strong in-plane carbon-carbon force constant, while the latter is related to the weak interplane one.[25,26] In regular bulk graphite, the scattering time associated with the in-plane acoustic phonons is estimated to be 10^{-12} s around room temperature, giving a mean free path of about 10^2 nm,[27] which is more than one order of magnitude larger than the particle size. This means that the in-plane phonon process that is dominant in ordinary regular graphite is not at work in the spin-lattice relaxation mechanism in graphite nanoparticles.

Next we discuss the longitudinal out-of-plane phonon mode as a plausible candidate, due to its energy range $\sim$200 K. The elongation of the intersheet distance in graphite nanoparticles reduces the strength of the intergraphene sheet interaction to a considerable extent, as already mentioned.[14] This results in a softening of the phonon mode. Moreover, the phonon energy spectrum is expected to be featured by discrete energy levels since only a small number of graphene sheets (3–6 sheets) participate in the graphite nanoparticle. Therefore, the excitation of the low-energy phonons, taking place even at low temperatures, is expected to contribute to the spin-lattice relaxation process. However, the estimated scattering time τ_p (Ref. 28) is still orders of magnitudes larger than the value ($\sim 10^{-15}$ s) obtained from the experimental result with Eq. (7). Thus an ordinary electron-phonon mechanism of Elliott type, that is related to the acoustic phonons of graphite, is ruled out as an explanation for the temperature dependence in the ESR linewidth.

Here emerges another plausible mechanism related to the nonbonding π electrons of the edge states which is not mediated through the acoustic phonons. The potentials of the peripheral atoms, around which nonbonding π electrons are localized, work to scatter conduction π electrons, and are able to participate in the spin-lattice relaxation process. Meanwhile, there exist Wallis-type local phonon modes associated with the vibrations of peripheral carbon atoms incorporated with foreign atoms or cross-linked carbon atoms attached to the edges of graphene sheets.[29–31] If a conduction electron interacts with an atom in which an electron of a nonbonding edge state is localized, the duration time for a scattering event is estimated at $t_d \approx 2 \times 10^{-16}$ s from the relation $t_d \approx r/\nu_F$ where the force range r of the interaction between the atom and a conduction electron is assumed to be $\sim$0.2 nm. The spin-lattice relaxation time associated with the interaction is given by the equation[32]

$$\frac{1}{T_1} \approx \frac{2 t_d}{\pi} \left(\frac{|H_{so}|}{\hbar} \right)^2, \tag{9}$$

where H_{so} is the Hamiltonian for the spin-orbit interaction of the atom having a localized nonbonding state, whose magnitude is in the range of the spin-orbit coupling λ. In this mechanism, where local phonons work as a reservoir, the interaction between electrons in the nonbonding band and the phonons gives a temperature dependence to the spin-lattice relaxation time. Equation (9) gives an estimate of $T_1 \approx 10^{-8}$ s for the spin-orbit coupling of carbon $\lambda \approx 14$ cm^{-1},[33] which is roughly comparable to that observed in the temperature-dependent term of the ESR linewidth. Consequently, the scattering of conduction electrons by the potentials of peripheral atoms having edge-inherited electronic and lattice dynamical features is the most plausible origin of the temperature-dependent spin-lattice relaxation process.

V. SUMMARY

Nanosized graphite particles are prepared through heat treatment of diamond nanoparticles with a size of 4–6 nm. Heat treatment at a temperature above 1600 °C converts diamond nanoparticles into graphite nanoparticles, and the elevation in the heat treatment temperature does not make the

particle size increase. According to the results of x-ray diffraction, Raman-scattering spectra, and transmission electron microscopy, the prepared graphite nanoparticle forms a polyhedron with a hollow inside it, whose faces comprise a stacking of 3–6 planar graphene sheets with the in-plane size of 7–8 nm and an intersheet distance of 0.353 nm. The intersheet distance is considerably larger than that for bulk graphite (0.3354 nm), resulting in a large reduction in the strength of interlayer interaction. ESR and magnetic susceptibility provide evidence of a considerable enhancement in the density of states at the Fermi energy. This fact means the presence of an additional band superimposed upon the bonding π and the antibonding π^* bands around the Fermi energy. Taking into consideration the discontinuous shape at edge lines formed by crossing adjacent graphene sheets, graphene sheets in a nanographite particle have open π-bond edges. In general, the periphery of a finite-size graphene sheet consists of zigzag- and armchair-type edges. Theoretical suggestions predict the formation of edge-inherited states having a nonbonding π-electron feature around the Fermi energy in the case of zigzag-type edges, where electrons in the states are mostly located around the marginal region of a graphene sheet. As a consequence, the enhancement in the density of states is suggestive of the contribution of the edge states in the electronic structure of nanosized graphene with open π-bond edges. This interesting electronic feature is considered to be associated with the specific size of graphite nanoparticles. The ESR spin-lattice relaxation process governed by boundary scattering events of π electrons is suggestive of specific features associated with the small size of the particles as well.

ACKNOWLEDGMENTS

The authors express their sincere thanks to Professor Mitsutaka Fujita, Yoshiyuki Shibayama, Professor Ko Sugihara, Dr. Sumio Iijima, Professor V. L. Kuznetsov, and Professor A. S. Kotosonov for their valuable discussions. Most importantly, our discussion with the late Professor Fujita gave us an important clue for explaining the magnetic behavior of graphite nanoparticles. The analysis of the ESR results is related to fruitful discussions with Professor Sugihara. O.E.A. and B.L.V.P. were supported by the Japan Science Promotion Society. This work was supported partly by Grants-in-Aid for Scientific Research Nos. 08404048, 09243209, and 09216205 from the Ministry of Education, Science and Culture, Japan.

*Author to whom correspondence should be addressed. Electronic address: tenoki@chem.titech.ac.jp

[1] M. S. Dresselhaus, G Dresselhaus, and P. C. Eklund, *Science of Fullerenes and Carbon Nanotubes* (Academic, San Diego, 1996).
[2] R. Kubo, J. Phys. Soc. Jpn. **17**, 975 (1962).
[3] S. J. Tans, M. H. Devoret, H. Dai, A. Thess, R. E. Smalley, L. J. Geerligs, and C. Dekker, Nature (London) **386**, 474 (1997).
[4] J. W. G. Wildoer, L. C. Venema, A. G. Rinzler, R. E. Smalley, and C. Dekker, Nature (London) **391**, 59 (1998).
[5] K. Tanaka, S. Yamashita, H. Yamabe, and T. Yamabe, Synth. Met. **17**, 143 (1987).
[6] M. Fujita, K. Wakabayashi, K. Nakada, and K. Kusakabe, J. Phys. Soc. Jpn. **65**, 1920 (1996).
[7] K. Nakada, M. Fujita, G. Dresselhaus, and M. S. Dresselhaus, Phys. Rev. B **54**, 17 954 (1996).
[8] M. Fujita, M. Igami, and K. Nakada, J. Phys. Soc. Jpn. **66**, 1864 (1997).
[9] A. M. Staver, N. V. Gubareva, A. I. Lyamkin, and E. A. Petrov, Fiz. Goreniya Vzryva **20**, 100 (1984).
[10] N. R. Greiner, D. S. Phillips, J. D. Johnson, and F. Volk, Nature (London) **333**, 440 (1988).
[11] T. Evans and P. F. James, Proc. R. Soc. London, Ser. A **277**, 260 (1964).
[12] L. S. Singer and J. Kommandauer, J. Chem. Phys. **34**, 133 (1961).
[13] D. S. Knight and W. B. White, J. Mater. Res. **4**, 385 (1989).
[14] H. Nagayoshi, Ph.D. thesis, University of Tokyo, 1975.
[15] V. L. Kuznetsov, I. Yu Malkov, A. L. Chuvilin, E. M. Moroz, V. N. Kolomiichuk, Sh. K. Shaichutdinov, and Yu V. Butenko, Carbon **32**, 873 (1994).
[16] V. L. Kuznetsov, A. L. Chuvilin, Yu V. Butenko, I. Yu Malkov, V. M. Titov, Chem. Phys. Lett. **222**, 343 (1994).
[17] D. Ugarte, Nature (London) **359**, 707 (1992).
[18] W. A. de Heer and D. Ugarte, Chem. Phys. Lett. **207**, 480 (1993).
[19] K. C. Pandey, Phys. Rev. B **25**, 4338 (1982).
[20] G. Kern, J. Hafner, and G. Kresse, Surf. Sci. **366**, 445 (1996).
[21] A. S. Kotosonov, Piz'ma Zh. Eksp. Teor. Fiz. **43**, 30 (1986) [JETP **43**, 37 (1986)].
[22] Y. Shibayama, H. Sato, T. Enoki, M. Endo, and N. Shindo, Mol. Cryst. Liq. Cryst. **310**, 273 (1998).
[23] B. T. Kelly, *Physics of Graphite* (Applied Science, London, 1981).
[24] R. Saito, Ph.D. thesis, University of Tokyo, 1984.
[25] K. Komatsu, J. Phys. Soc. Jpn. **10**, 346 (1955).
[26] K. Sugihara, Y. Hishiyama, and A. Ono, Phys. Rev. B **34**, 4298 (1986).
[27] K. Sugihara, Phys. Rev. B **28**, 2157 (1983).
[28] K. Sugihara, Phys. Rev. B **37**, 7063 (1988).
[29] F. Wallis, Phys. Rev. **116**, 302 (1959).
[30] M. Igami, Master's thesis, University of Tsukuba, 1998.
[31] M. Igami, M. Fujita, and S. Mizuno, Appl. Surf. Sci. **130-132**, 870 (1998).
[32] K. Sugihara (private communication).
[33] K. A. Müller and R. Kleiner, Phys. Lett. **1**, 98 (1962).